IOPscience iopscience.iop.org

Home Search Collections Journals About Contact us My IOPscience

Macroscopic electric field and osmotic pressure in ultracentrifugal sedimentation–diffusion equilibria of charged colloids

This article has been downloaded from IOPscience. Please scroll down to see the full text article.

2005 J. Phys.: Condens. Matter 17 2293

(http://iopscience.iop.org/0953-8984/17/15/004)

View the table of contents for this issue, or go to the journal homepage for more

Download details:
IP Address: 129.252.86.83
The article was downloaded on 27/05/2010 at 20:37

Please note that terms and conditions apply.

INSTITUTE OF PHYSICS PUBLISHING JOURNAL OF PHYSICS: CONDENSED MATTER

J. Phys.: Condens. Matter **17** (2005) 2293–2314 doi:10.1088/0953-8984/17/15/004

Macroscopic electric field and osmotic pressure in ultracentrifugal sedimentation–diffusion equilibria of charged colloids

M Rasa[1], B H Erné[1], B Zoetekouw[2], R van Roij[2] and A P Philipse[1,3]

[1] Van't Hoff Laboratory for Physical and Colloid Chemistry, Utrecht University, Debye Institute, Padualaan 8, 3584 CH Utrecht, The Netherlands
[2] Institute for Theoretical Physics, Utrecht University, Leuvenlaan 4, 3584 CE Utrecht, The Netherlands

E-mail: a.p.philipse@chem.uu.nl

Received 14 December 2004, in final form 22 February 2005
Published 1 April 2005
Online at stacks.iop.org/JPhysCM/17/2293

Abstract

Sedimentation–diffusion (SD) equilibria from analytical ultracentrifugation of well-characterized charged silica spheres in ethanol deviate strongly from a barometric profile and demonstrate the existence and substantial effects of a recently predicted internal macroscopic electric field (van Roij 2003 *J. Phys.: Condens. Matter* **15** S3569). Experimental SD-profiles yield the gradient of the electrostatic potential energy of the colloids, which clearly manifests an almost homogeneous macroscopic electric field. Electrochemical Donnan potential measurements confirm a difference in electrical potential between the top and bottom of the profiles. A 'non-barometric' limiting law derived from electroneutrality explains the trends in the SD-profiles quite well. Our analysis of osmotic pressures (obtained from integrating SD-profiles) beyond this simple law includes, among other things, colloid–ion attractions and extra volume terms in the free energy.

1. Introduction

The sedimentation–diffusion (SD) equilibrium of colloids corresponds to a concentration profile resulting from the competition between Brownian motion and sedimentation in a gravitational or centrifugal field. The SD-equilibrium is an important source of thermodynamic information about the colloids under study, because the profile is directly related to the osmotic equation of state. A classical example is Perrin's determination [1] of the Boltzmann constant

[3] Author to whom any correspondence should be addressed.

 © 2005 IOP Publishing Ltd Printed in the UK

from a measured SD-profile of non-interacting colloids in a gravitational field. For non-interacting colloids the profile is expected to be an exponential Boltzmann distribution (the 'barometric profile'), so for colloids of known weight, the Boltzmann constant is obtained from a logarithmic plot of colloid number density versus height. Conversely, the thermal energy kT is the only parameter needed to determine an unknown colloid weight, provided that the SD-profile is the barometric profile expected at sufficiently low colloid densities. This expectation is in general only justified for uncharged colloids: for charged colloids [2–9] pronounced deviations from the barometric profile may occur even at very low colloid concentrations.

This non-barometric behaviour is explained by recent theory [2, 5] and simulations [6] as a manifestation of a macroscopic electric field in the SD-profile which reduces the effective colloidal mass. In a recent experimental study on charged silica spheres in ethanol [4], the presence of an electric field was mentioned as one of the few options left to explain the enormous spatial extension of SD-profiles of the colloids under study, even at the very low densities where only a barometric distribution on a much smaller length scale was expected. Deviations from the barometric profile and the possibility of an electric field have been reported earlier for charged latex spheres at high ionic strength [7]. Biben and Hansen [2] and van Roij [5] have provided the first clear theoretical explanation of the electric field and its effect on SD-profiles, an effect which may be drastic, as is also confirmed by recent simulations [6]. Reference [5] analyses the three characteristic regions that can be identified [5] in the gravitational SD-profile: region I—an exponential tail of the profile with a decay length as if particles were uncharged (the 'barometric' part); region III, which is also an exponential one but with a decay length increased by a factor of the order of z (the colloidal charge); and an intermediate region II, where, quite surprisingly, the concentration profile is *linear* in height. A homogeneous electric field is predicted to be present in regions II and III (in region I it is negligible), where the colloids are lifted upwards against gravity. In region II, it is argued [5], the effective colloid mass is nearly zero because there the electric field almost cancels the very gravity that causes its existence. Reference [5] derives separate expressions for the three regions from the Donnan equilibrium, supplementing the analysis by including the electrical (Maxwell) stress in the force balance on the particles to account for the charge separation (formation of a macroscopic condenser), responsible for the homogeneous electric field in regions II and III. It has also been shown [8] that the Donnan equilibrium, without any additional assumptions, entails limiting laws for both the entire SD-profile and the accompanying electric field containing the three regions referred to above as asymptotic solutions.

Recently the first experimental evidence for the existence and effects of the electric field was reported in an analytical ultracentrifugation (UC) study on SD-profiles of charged silica spheres in ethanol [9]. In the present paper, we not only present additional UC measurements on the same silica dispersions but also provide a more extended analysis of SD-profiles to obtain, among other things, the osmotic pressure as a function of silica concentration. Moreover, since the electric field is identified [5, 8] as a gradient in the Donnan potential, it is clearly of interest to compare the overall electric potential jump determined from the SD-profiles to direct electrochemical measurements of the Donnan potentials of silica dispersions. Such measurements have not been performed earlier, so in the experimental section 3 Donnan potential measurements on silica alcosols are explained in some detail. In section 2 we recapitulate a derivation of the non-barometric SD-profile in a centrifugal field [8, 9] also to illustrate that it is a limiting law which solely relies on the assumptions of macroscopic charge neutrality for colloids plus ideal ions. Results are discussed in section 4, for reasons of clarity figure by figure, followed by a general discussion in section 5, which also includes a comparison between experimental equations of state of the silica spheres, to osmotic pressure calculations beyond the model outlined below.

2. Non-barometric SD-profiles

Sedimentation of charged colloidal particles involves both colloids and ions in the dispersion which form a system of three interpenetrating fluids, or a mixture of three species, namely colloidal particles with number density ρ each carrying z elementary charges, monovalent cations with concentration c_+, and monovalent anions with concentration c_-. The dispersion is in osmotic equilibrium with a large salt reservoir with a total ion concentration $2c_s$. At equilibrium, the forces acting on any volume element of the three fluids must be in balance for each fluid. Here we consider sedimentation in a centrifugal field; the case of gravitational settling is discussed in [5, 8]. Because of the huge mass difference between ions and colloids, the centrifugal field produces spatial separation between them, which is responsible for the formation of the macroscopic electric field.

The effect of the centrifugal field on ions is negligible (in comparison to that on colloids), so the equilibrium condition for ions is:

$$-kT\frac{\mathrm{d}c_\pm}{\mathrm{d}r} \pm ec_\pm E = 0, \tag{1}$$

where E is the internal macroscopic electric field, related to the electrostatic potential ψ by $E = -\mathrm{d}\psi/\mathrm{d}r$, r is the radial coordinate, and e is the proton charge. Introducing the dimensionless electrostatic potential:

$$\phi = \frac{e\psi}{kT}, \tag{2}$$

the distribution of ions in the SD profile, given by equation (1), becomes:

$$c_\pm = c_s \exp(\mp\phi). \tag{3}$$

For the case of the much heavier colloids, the equilibrium equation is:

$$-kT\frac{\mathrm{d}\rho}{\mathrm{d}r} - ze\rho E + m_c\rho\omega^2 r = 0, \tag{4}$$

where m_c is the particle mass corrected for buoyancy and ω is the angular frequency of rotation. We remark that the electric field term in equation (4) must be accompanied by the centrifugal field term: if the centrifugal field vanishes, the electric field must vanish too. To derive the colloid profile from equation (4), one more equation is needed, which we find from the macroscopic neutrality condition (the colloid charge is negative as in the experiments):

$$-z\rho + c_+ - c_- = 0. \tag{5}$$

By combining equations (3) and (5) one obtains:

$$y = -\sinh(\phi), \tag{6}$$

where y is the non-dimensional number density of colloidal particles:

$$y = \frac{z\rho}{2c_s}. \tag{7}$$

From equation (6) it clearly follows that an electric field is only present in the case of a sedimented dispersion, i.e., for a concentration profile of colloidal particles. The validity of the neutrality condition (5) holds for volumes much larger than the volume with dimensions of the order of the Debye screening length. Equation (5) is macroscopic and is consistent with the (macroscopic) fluid model, but it disregards details in the electric fields on a local scale comparable to the Debye length. Using the neutrality condition in the fluid equations, but assuming (on a smaller scale) $\nabla \cdot E \neq 0$, is known as the plasma approximation [10]. The presence of an electric field due to charge separation, incidentally, is well-known in plasma

physics: a typical plasma consists of electrons and ions, which have very different masses. The electric field appears in various phenomena like wave propagation and ambipolar diffusion [10].

From equations (4) and (6), after integration, the equation for the SD-profile is found to be:

$$\ln(y) + z\,\mathrm{arcsinh}(y) = \frac{r^2}{2L_\omega^2} + \text{const.} \tag{8}$$

L_ω is the so-called centrifugal length given by:

$$L_\omega = \left(\frac{kT}{v(\rho_\mathrm{p} - \rho_\mathrm{s})\omega^2}\right)^{\frac{1}{2}}, \tag{9}$$

where ρ_p is the mass density of the colloidal particles, ρ_s is the mass density of the solvent, and v is the volume of one particle. The non-barometric term $z\,\mathrm{arcsinh}(y)$ in equation (8) is the direct contribution of the electric field to the profile and adds to the barometric term $\ln(y)$, just as in the case of one-dimensional sedimentation under gravity [8]. Only if the former term is negligible does the barometric profile hold (see equation (10)), and L_ω has the meaning of the effective spatial extension of the profile. The three regions found in [5] are asymptotic solutions of the equivalent of equation (8) for gravitational settling [8]. For a centrifugal field, they are given by:

$$\rho_\mathrm{I}(r) \sim \rho_\mathrm{I}(r_1)\exp\left(\frac{r^2 - r_1^2}{2L_\omega^2}\right), \qquad r < r_1 \tag{10}$$

$$\rho_\mathrm{II}(r) \sim \rho_\mathrm{II}(r_1) + \frac{r^2 - r_1^2}{z^2 L_\omega^2/c_\mathrm{s}}, \qquad r_1 < r < r_2 \tag{11}$$

$$\rho_\mathrm{III}(r) \sim \rho_\mathrm{III}(r_\mathrm{b})\exp\left(\frac{r^2 - r_\mathrm{b}^2}{2(z+1)L_\omega^2}\right), \qquad r_2 < r < r_\mathrm{b}. \tag{12}$$

The three regimes, referred to as region I, II, and III, occur under the following conditions [5]. Region I is the barometric profile and it corresponds to the case $zy < 1$. The intermediate region II is in the centrifugal field a parabola and occurs if $zy > 1$ but $y < 1$. The third region is also exponential but with an inflated decay length in comparison to that of the barometric exponential and can be observed experimentally if $y > 1$. In equations (10)–(12) r_1 and r_2 are the crossover coordinates between the regions I and II, and II and III, respectively. In equation (12) we prefer to use r_b instead of r_2, where r_b is the radial coordinate of the bottom of the centrifuge sedimentation cell. Given that the crossover coordinates r_1 and r_2 are such that $y(r_1) = 1/z$ and $y(r_2) = 1$, we can write:

$$\frac{y(r_2)}{y(r_1)} = z, \tag{13}$$

which provides an alternative to estimate the particle charge and at the same time a possibility of verifying the fitting results. We note here that the $1 + z$ reduction of the molar mass as in region III was already discussed by the pioneers of ultracentrifugation (Svedberg, Tiselius; see the brief historical review in [8]).

In our experiments, the salt reservoir is actually the top of the profile (referred to as the supernatant), which has a very low particle concentration and occupies a significant part of the sedimentation cell. Initially, samples without added salt were measured. The total ion concentration in the supernatant is identified as $2c_\mathrm{s}$ and can be calculated by extrapolating the measured colloid volume fraction (Φ) dependence of the ion concentration to $\Phi = 0$. The presence of ions in our dispersions is mainly due to ionization of colloid surface groups and dissociation of solvent molecules, supplemented by residual ions resulting from the chemical

Table 1. Properties of charged silica spheres (SiA) dispersed in ethanol.

R^a (nm)	p (%)	$R_h{}^b$ (nm)	δ^c (g cm^{-3})	μ^d (μm cm V^{-1} s^{-1})	z^e
21.9	11.6	30.0	1.6($\pm$0.1)	$-0.1(\pm0.10)$	$\approx$50

[a] Radius and p the polydispersity of particles measured from transmission electron microscopy.
[b] Radius from dynamic light scattering.
[c] Mass density from [29].
[d] Electrophoretic particle mobility for silica volume fractions in the range 0.015%–0.48%.
[e] Number of elementary charges on silica particles, estimated from electrophoretic mobility.

synthesis of the silica dispersion. The concentration of ions of the latter type was minimized by dialysis of the stock dispersion against pure ethanol.

3. Experimental details

3.1. Colloidal dispersions

Dispersions of negatively charged silica particles (SiA) in ethanol were investigated at different silica volume fractions Φ and at low ion concentration $2c_s$, as well as at fixed volume fraction of particles ($\Phi = 0.3\%$) with increasing amounts of added salt ($LiNO_3$). Amorphous silica spheres, with properties presented in table 1, were synthesized by polymerization of (hydrolyzed) tetraethoxysilane in an ethanol–ammonia mixture [11]. The silica surface was modified by covalent reaction with 3-methacryloxypropyltrimethoxysilane (TPM) during distillation, simultaneously transferring the silica spheres to absolute (analytical grade) ethanol [11]. The stock dispersion for the ultracentrifugation experiments was free from contaminants such as polymeric species or secondary silica particles, which might affect SD-profiles [4]. TPM-coated silica spheres do not aggregate in ethanol and are well-documented model particles for the study of charge-stabilized colloids [11, 12]. Particle characterization (table 1) was performed on the same samples as used for ultracentrifugation. The dynamic light scattering radius in table 1 is larger than the TEM-radius because the former includes the (solvated) TPM-layer which is invisible for TEM. Moreover, silica spheres tend to shrink in the electron microscope, and also polydispersity enhances the light scattering radius.

We have also measured the sedimentation profiles of uncharged particles for comparison. Commercially available silica particles (Ludox HS-40, DuPont), initially dispersed in water, were coated with octadecylalcohol and redispersed in cyclohexane as described elsewhere [13]. The average radius of these particles, determined from dynamic light scattering measurements, is 18 nm.

3.2. Experimental techniques

Analytical ultracentrifugation. Ultracentrifugation was performed using a Beckman Optima XL-A analytical ultracentrifuge and sector-shaped sedimentation cells, thermostatically controlled at $T = 298.0$ K. The ultracentrifuge is equipped with an optical scanning system, which measures the transmittance H through the sample relative to a reference of pure ethanol as a function of the radial coordinate at a chosen wavelength. The results are converted to attenuance A defined by $A = \ln(1/H)$. The attenuance (also known as extinction) is in our case due to the Rayleigh scattering by silica particles, as confirmed by wavelength scans: the attenuance varied with λ^{-4}, where λ is the wavelength of the incident light. Consequently, the range of linear dependence of attenuance on the particle volume fraction Φ is limited due to the influence of the structure factor at higher concentrations. Our measurements (figure 1)

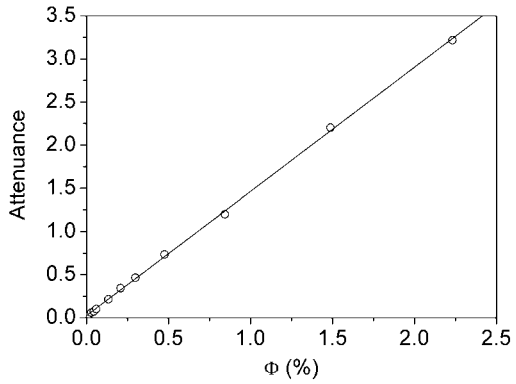

Figure 1. Attenuance measured by the analytical ultracentrifuge for different volume fractions of colloids at a wavelength of 325 nm. Up to 2.5 vol% a linear dependence is observed.

show that the linear dependence is valid up to silica volume fractions of approximately 2.5%. Consequently, only for profile segments with volume fractions below 2.5% is a direct conversion to silica concentration possible. For samples with an initial volume fraction up to 0.5% (that is the volume fraction of the homogeneous sample before centrifugation) the whole profile can be rescaled in terms of particle number density by determining the extinction coefficient from figure 1. At higher initial volume fractions, only the upper part of the profiles can be rescaled in this manner.

A first series of measurements was performed at 1100 rpm (which corresponds to an acceleration of $88g$ in the centre of the cell) for a period of up to 7 days to achieve equilibrium profiles of sufficient thickness, which nevertheless fully decay within the available (radial) space to the supernatant depleted of particles (within the limits of the instrument accuracy). The state of equilibrium was checked by subtracting the data recorded at intervals of 24 h. The reproducibility of the profiles was very good (a few per cent) when the measurements were repeated after the cell content was homogenized by stirring it for 15 min. This reproducibility also confirms that the silica spheres do not aggregate in the centrifugal field.

A second series of measurements was performed at 2200 rpm for low volume fraction samples and even at higher rotation velocities for more concentrated samples.

Donnan potential measurements. Donnan potential measurements, in particular on non-aqueous dispersions, are rather uncommon. Therefore we describe experimental aspects of the method in detail, referring to Overbeek [14, 15] and Lyklema [16] for extensive discussion of theoretical aspects. The aim is to measure the electrical potential difference between the top and bottom fractions of a centrifuged dispersion, using two electrodes to probe the electrical potentials.

Salt bridges are necessary for the electrochemical measurement of Donnan potentials [14, 15]. An incorrect approach would be to measure the voltage between two reversible electrodes without salt bridges, for instance two platinum electrodes, because the potential difference between two reversible electrodes must be zero at thermodynamic equilibrium [14–17] (a reversible electrode is one for which electron transfer is unimpaired to and from the electrolyte solution, so that the electrode potential is completely determined by the composition of the electrolyte solution [15]). A major drawback of salt bridges, however, is that they contaminate the sample dispersions with salt, causing a decrease of the Donnan potential. In our experiments, the salt bridge solutions leaked at about 5 μl h^{-1} into the

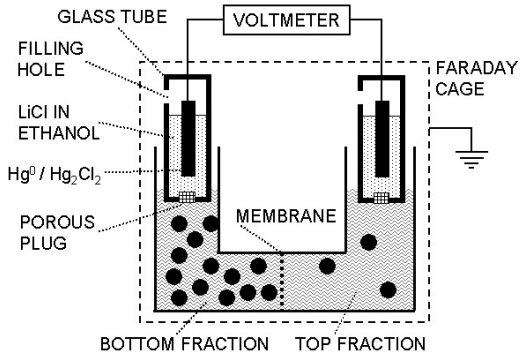

Figure 2. Schematic illustration of the setup used to measure Donnan potentials.

samples. This is quite a complication, because (a) our sample volumes are small, (b) their salt concentrations are very low ($\approx$30 μM) and must remain unchanged, and (c) the maximum expected signal is small, of the order of 10 mV, so that weak artefacts may have an important influence on the measurements.

One way to limit contamination of the samples is to use dilute salt bridge solutions. However, unless salt bridge solutions are much more concentrated than the sample dispersions under study (at least by a factor of 10), the liquid junction potentials at the salt bridges may dominate the measured potential [17–21], thwarting the measurement of the Donnan potential. These liquid junction potentials result from different concentrations and mobilities of the ions. Another way to limit salt contamination is to minimize the leakage rate, although 'a constant and substantial flow rate is probably the most critical factor for obtaining reproducible junction potentials' [18]. Moreover, the leakage rate also affects the measurement by causing a streaming potential, approximately proportional to the flow rate [15, 16, 21–23]. Such a streaming potential arises from the pressure applied on the porous plug at the bottom of the salt bridge by the column of salt bridge solution, causing a flow of the mobile part of the electrical double layer at the surface of the capillaries in the porous plug relative to the stationary part of the double layer. Preliminary experiments indicated a dependence of 1 mV cm^{-1} on the height of the column of salt bridge solution.

In our measurements, we attempted to equalize the leaking rates of the two electrodes, by using two commercial electrodes of the same type, filled to the same height with the same salt solution, and introduced at the same height in the two sample dispersions. To evaluate the effect of differences in liquid junction potential between the two electrodes, their salt bridges were filled with a series of different LiCl concentrations ranging from 10 μM to saturation. Each time the LiCl concentration of the two salt bridges was changed, a constant potential difference between the two electrodes in a salt solution was obtained after a few days of equilibration. Before and after measuring the sample dispersions, their conductivity was measured, to evaluate the effect of leakage from the salt bridges. Another measure taken to equalize the liquid junction potentials of the electrodes was to employ salt bridge solutions made from the same solvent as the sample solutions; using a different solvent would have an unpredictable, possibly large effect [24].

Figure 2 gives a schematic illustration of our setup for measuring Donnan potentials. The voltage was measured between two ethanolic calomel electrodes [25, 26]. Each electrode, prepared by removing the aqueous salt bridge solution of a REF921 from Radiometer Analytical, consisted of a glass tube containing a calomel-covered mercury element immersed

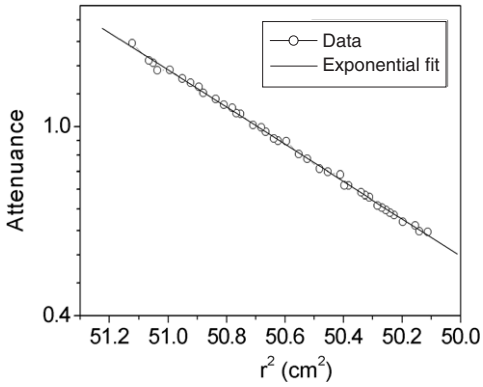

Figure 3. Profile produced by uncharged silica particles SiL in cyclohexane with an initial volume fraction of 0.2%. The measured attenuance is plotted versus the radial coordinate with the origin in the centre of rotation. As expected, the profile is barometric.

in a solution of LiCl in ethanol (which will be referred to as 'salt bridge'); the LiCl solution could be replaced through a filling hole and was in contact with the sample dispersion by way of a porous plug (a pin consisting of silicoaluminates with pore sizes in the range 1.2–1.5 μm). The mercury was in contact with the external electrical circuit (the mercury was contained in a smaller concentric internal glass tube with a second porous plug, not shown in figure 2). The two calomel electrodes were introduced in two sample dispersions separated by a dialysis membrane (Spectra/Por Type 6, MWCO:50000, Biotech). Screw-caps were used to prevent loss of ethanol from the samples due to evaporation. Voltages were measured using the electrometer of an Autolab electrochemical instrument (Eco Chemie, input impedance >100 GΩ). The membrane cell and the electrodes were in a grounded Faraday cage, which is crucial for reliable measurements.

The dispersions in the two sample compartments were 3 ml fractions from the top and bottom of a 0.2 vol% silica dispersion (SiA, see table 1) centrifuged for 2 h at 7000 rpm (acceleration: 6000g; total volume: 35 ml) in a preparative ultracentrifuge. In this way, the bottom fraction had a background salt concentration of the same order as the top fraction but a silica concentration higher by about a factor of 10.

Electrophoresis and electrical conductivity measurements were performed with a DELSA 440SX (Coulter) at $T = 298$ K on the same samples used in the ultracentrifuge. In the case of electrophoretic measurements, the samples were filtered prior to the measurements to remove dust. The mobility was determined from a Lorentzian fit to the measured peaks at four scattering angles and further used to estimate the number of elementary charges z of the particles as described in section 4. Conductivities obtained from DELSA were used to estimate the total concentration of ions.

4. Results

4.1. Analytical ultracentrifuge measurements

In this section, experimental data are discussed in terms of the non-barometric law equation (8), in particular on the basis of its asymptotic forms equations (10)–(12). A more general discussion beyond the validity of equations (10)–(12) follows in section 5.

For the case of the uncharged silica particles SiL in cyclohexane, the expected barometric profile (equation (10)) is obtained (figure 3), with a centrifugal length in reasonable agreement

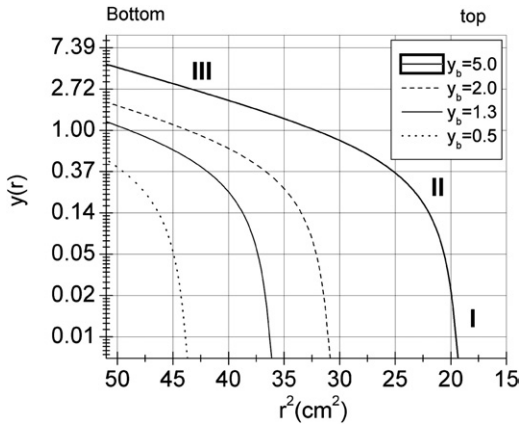

Figure 4. Non-dimensional concentration profiles predicted by equation (8). y_b is the non-dimensional concentration at the bottom of the cell ($r_b = 7.15$ cm). The centrifugal length is $L_\omega = 0.36$ cm and the charge $z = 50$. These numerical values correspond to the values encountered in our measurements.

with the colloid weight. For the case of the charged silica spheres SiA in ethanol, all measured profiles deviate from the barometric one. An example of theoretical prediction for the effect of the internal macroscopic electric field on profiles in a centrifugal field, according to equations (10)–(12), is presented in figure 4. The centrifugal length and charge of particles correspond to our particles (see below). At high enough volume fraction of colloids and low salt concentration, all three regions are seen in one and the same profile. The region III expands when the volume fraction of colloids increases; the same behaviour is predicted if the volume fraction is fixed but the salt concentration decreases.

In figure 5(a), the measured profiles at very low initial volume fractions of SiA particles at 1100 rpm are presented. For the sample with an initial silica volume fraction of 0.015%, further referred to as the '0.015% sample', the barometric part of the profile (region I) dominates, but nevertheless a significant deviation is observed close to the bottom of the cell. The non-barometric part of the profile for this sample as well as for the 0.030% sample are not well described by equations (11) and (12). However, in the case of the 0.045% sample, all three regions expected from equations (10)–(12) can be clearly distinguished in the profile.

The barometric part of these three curves yields practically the same centrifugal length L_ω (see table 2). For the mass density of silica in table 1, equation (9) yields an average particle radius of 19.3 nm. This value is smaller than the average TEM radius by 12%, probably because the smaller particles of the size distribution are present in the top of the profile (which has to be used for the determination of L_ω).

The regions II and III of the 0.045% sample were fitted with equations (11) and (12), respectively, to find the number of elementary charges z on the colloids (further referred to as particle charge). From region III, the charge $z^{(\mathrm{III})}$ is determined directly as a fit parameter, using the value of L_ω from region I (see table 2). The values of L_ω determined from region I of each profile, incidentally, are used in all cases discussed in this paper.

From region II, $z^{(\mathrm{II})}$ can be determined if the measurements are rescaled in terms of particle number density ρ, and if the ion concentration in the supernatant $2c_s$ is known. The determination of the crossover coordinate r_1 was done directly from the logarithmic plot. The particle number density is determined by using a calibration plot appropriate for this sample (like the one in figure 1 but at $\lambda = 240$ nm), and volume fraction of particles written as $\Phi = \delta v$. The volume of a particle v was calculated using the average TEM diameter. The

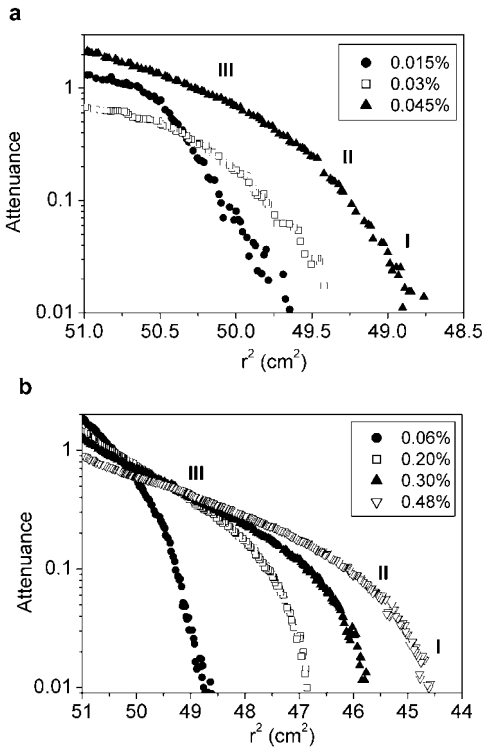

Figure 5. ((a), (b)): Experimental sedimentation–diffusion equilibrium profiles of charged silica spheres SiA plotted as attenuance versus the square of the radial coordinate, for different volume fractions of particles.

Table 2. Electrical conductivity, total ion concentration, Debye length, and results of profile analyses for charged silica particles SiA.

Φ^{a} (%)	σ^{b} (μS cm^{-1})	$c_{tot}{}^{c}$ (10^{-5} M)	$\kappa^{-1\,d}$ (nm)	$L_{\omega}^{(I)\,e}$ (cm)	$z^{(II)\,f}$	$z^{(III)\,g}$	$y(r_2)/y(r_1)^{h}$
0.015	1.30	1.66	59	0.36	—	—	—
0.03	1.36	1.73	58	0.37	—	—	—
0.045	1.43	1.82	56	0.36	30	3	4
0.06	1.55	1.97	54	0.36	27	3	4
0.13	1.78	2.27	50	0.37	34	4	6
0.2	2.00	2.55	47	0.39	34	4	5
0.3	2.33	2.97	44	0.39	38	5	4
0.48	2.92	3.72	39	0.37	40	8	7

[a] Initial volume fraction of particles.
[b] Electrical conductivity.
[c] Total ion concentration estimated from conductivity measurements.
[d] Debye length.
[e] Centrifugal length determined from region I of profiles.
[f] Number of elementary charges of particles determined from region II of the profiles.
[g] Number of elementary charges of particles determined from region III of the profiles.
[h] Ratio of non-dimensional particle concentrations at the crossovers between the three regions.

total ion concentration for the homogeneous dispersion was estimated from:

$$c_{tot} \approx \frac{\sigma}{e(\mu_+ + \mu_-)}, \tag{14}$$

where σ is the electrical conductivity. This simple equation is expected to give at least the correct order of magnitude when both the ion concentration and the particle concentration are very low. Consequently, the proton mobility in ethanol at infinite dilution $\mu_+ = 6.1 \times 10^{-8}$ m^2 V^{-1} s^{-1} was used, and an order of magnitude for the mobility of negative ions $\mu_- \approx 2 \times 10^{-8}$ m^2 V^{-1} s^{-1} was assumed. The results are presented in table 2. We do not expect more than the correct order of magnitude from equation (14). We may have different types of ions in our sample—see the discussion in section 2: protons with concentration c_H^+ (counterions) produced by the colloids as well as positive and negative ions with concentrations c_p and c_m (assumed monovalent) so that $c_p = c_m \neq c_{H^+}$. Consequently, we have $\sigma = e(c_{H^+}\mu_+ + c_p\mu_- + c_m\mu_-)$. If we assume an average mobility of ions $\langle\mu_i\rangle$ for these three species, then the total ion concentration is $c_{tot} = \sigma/(e\langle\mu_i\rangle)$, which agrees in order of magnitude with equation (14). The total ion concentration c_{tot} was estimated from conductivity data for all analysed samples (see table 2). From extrapolation to $\Phi = 0$, the value $2c_s \approx 16\ \mu$M was obtained.

The charge z was estimated from electrophoretic mobility measurements, using the Debye–Hückel approximation [27], according to [28], from the equation:

$$ze = 4\pi\varepsilon_0\varepsilon_r|\zeta|R(1 + R\kappa), \tag{15}$$

where ε_0 and ε_r are the electrical permittivities of vacuum and ethanol respectively. This method is justified because of the relatively small radius R of particles and large Debye length κ^{-1}, as shown below. We replaced here the surface potential by the zeta potential ζ, which is a reasonable approximation since the electrical potential around silica spheres in ethanol decays only weakly because of the large Debye length. The zeta potential was determined in our case from Hückel's equation: $\zeta = 3\mu\eta/(2\varepsilon_0\varepsilon_r)$. Here μ is the measured electrophoretic mobility of particles (see table 1) and η the viscosity of solvent. We found $\zeta = -76.6$ mV. Using the total ion concentrations obtained with equation (14), the Debye length was estimated from $\kappa^{-1} = [\varepsilon_0\varepsilon_r kT/(e^2 c_{tot})]^{1/2}$ (see table 2). Since $\kappa R < 1$, a reasonable estimation of the particle charge via equation (15) and Hückel's equation can be expected. The measured electrophoretic mobility was practically independent of the volume fractions of particles. Consequently we assume the value $z \approx 50$, determined from the 0.3% sample, as the order of magnitude of particle charge for all samples in this study.

Finally, the ratio $y(r_2)/y(r_1)$ of the non-dimensional particle number densities (see equation (13)) at crossovers was estimated from figure 5(a) and is presented in table 2.

The profiles obtained for SiA colloids at slightly higher concentrations, centrifuged at 1100 rpm, are presented in figure 5(b). They all show the three regions in each profile, in very good qualitative agreement with equations (10)–(12). An example of the very good fits of the data in the region II and III with equations (11) and (12), respectively, is given in figures 6(a), (b). The determined values of L_ω, $z^{(II)}$, and $z^{(III)}$ for each sample are presented in table 2. In the case of the 0.48% sample, region III shows a small distortion anticipating the results presented in figure 9 (see below).

At increasing salt concentration, the effect of the internal electric field is progressively reduced (together with the extent of regions II and III) until the barometric part dominates the profile (figure 7). Note that only little salt is needed to change the profiles substantially.

We will now process the experimental SD-profiles further to obtain explicit information about the electric field as proposed in [8]. The barometric exponential part is present in all experimental profiles, so it can be easily extracted from the data by multiplying the normalized non-dimensional profile $y(r)/y(r_b)$ by $\exp[-(r^2 - r_1^2)/(2L_\omega^2)]$, where $y(r_b)$ is the non-dimensional concentration of particles at the bottom of the cell. If equation (8) holds, the logarithm of this product should equal $z\phi$. The results for three volume fractions are

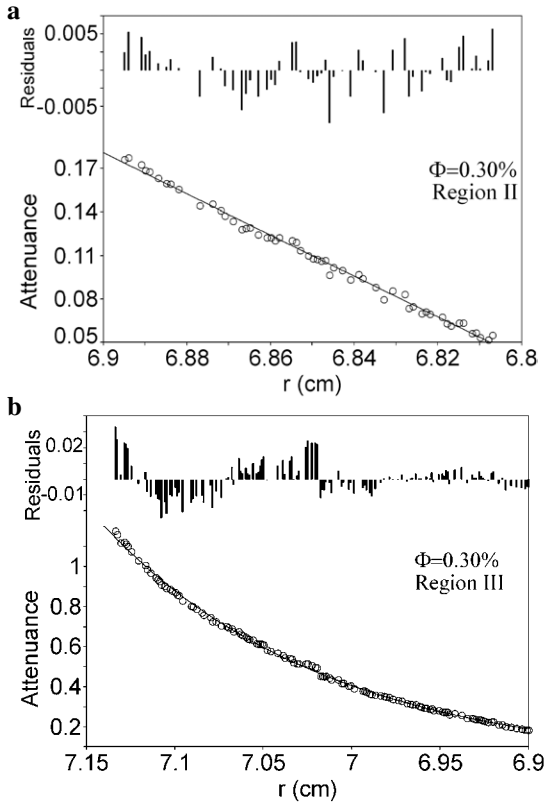

Figure 6. Examples of fit analysis of the experimental profile of the 0.30% sample (figure 5). (a) A nearly perfect quadratic fit to the data extracted from region II, which clearly confirms the decay predicted for this region (see equation (11)). (b) A nearly perfect exponential fit to the data extracted from region III of the same sample (see equation (12)), resulting in a different centrifugal length than that of region I.

presented in figure 8(a), clearly manifesting the linear change in ϕ, i.e., the homogeneous electric field. Corresponding to the region III of the profile, in the limit $z \gg 1$, one obtains the following equation:

$$z\phi^{(\mathrm{III})} \approx -\frac{r^2 - r_\mathrm{b}^2}{2L_\omega^2}. \tag{16}$$

It can be seen from figure 8(a) that the curves superimpose close to the bottom of the cell while they flatten at different levels upon entering the region I, where the electrical potential approaches its constant value in the supernatant. Equation (16), in principle, provides the electrostatic potential ϕ if z is accurately known from separate measurements. Taking into account the relationship between the electrostatic potential and field strength, the ratio between the electric and centrifugal force acting on a colloidal particle becomes:

$$\frac{zeE}{m_\mathrm{c}\omega^2 r} = -\frac{L_\omega^2}{r}\frac{\mathrm{d}(z\phi)}{\mathrm{d}r}. \tag{17}$$

Using the slope of the quasi-linear region III as plotted in figure 8(a), equation (17) yields a value close to unity for the ratio of the two forces, as expected from the discussion in [5]: the

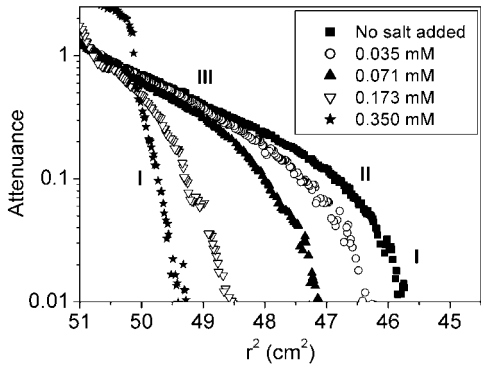

Figure 7. Representative experimental profiles for dispersions having a fixed initial silica volume fraction of 0.30%, at different salt concentrations. The total ion concentration is obtained by multiplying the salt concentration by 2. The background ion concentration is of the order of 0.016 mM. Increasing added amounts of $LiNO_3$ gradually compress the profile towards the barometric distribution I.

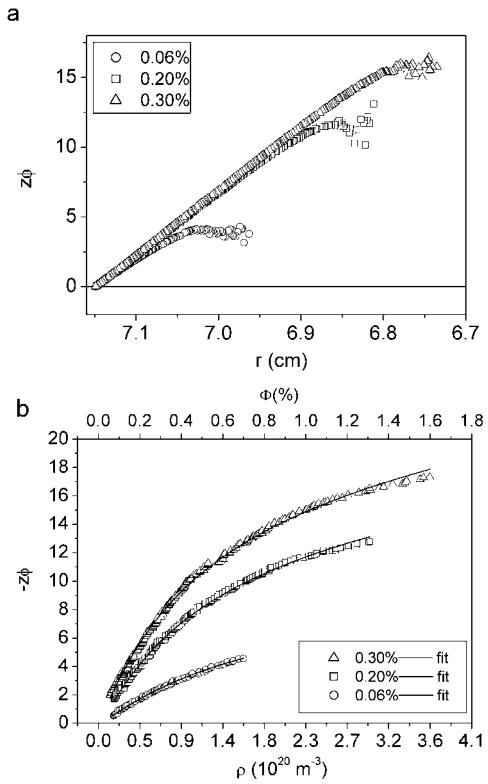

Figure 8. The non-dimensional potential energy of particles in sedimented dispersions versus (a) the radial coordinate, (b) the particle number density. The electrical potential gradient clearly shows the presence of an electric field as a function of r, which is quasi-homogeneous in the region III of profiles. Equation (6) was used to perform the fit in plot (b).

electric field indeed virtually balances the weight of the colloids in the centrifugal field. Note that the value of z is not needed for the evaluation of this force ratio.

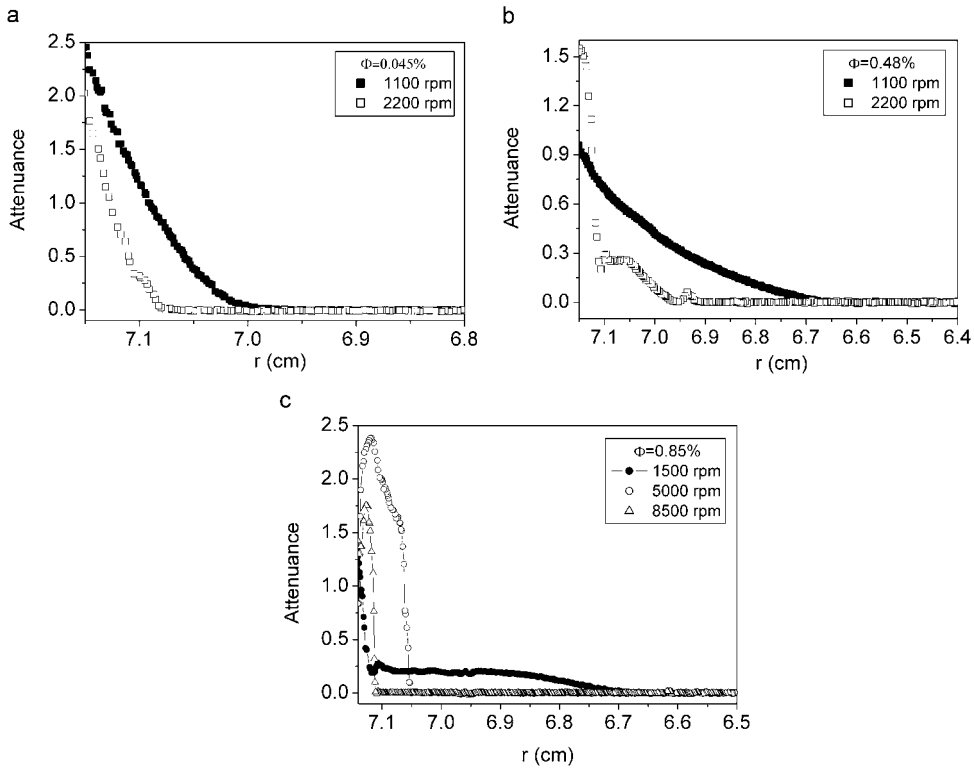

Figure 9. Examples of profiles which deviate from that described by the theoretical model (equations (10)–(12)). ((a), (b)) Profiles measured for some of the samples also presented in figure 5, but at a higher rotation velocity. (c) Profiles measured for a more concentrated sample at different rotation velocities.

By identifying the particle concentration corresponding to each value of r, we can convert figures 8(a) to (b). The curves do not overlap in this case since the initial slope (see equation (6)) depends on z^2, which (if equations (11) and (12) are correct) apparently depends on the volume fraction (see table 2).

When the sedimentation equilibrium measurements were performed at 2200 rpm, the shape of SD-profiles clearly changed (figures 9(a), (b)). The changes are substantial at higher initial volume fractions of colloids, as can be seen in figure 9(b), which shows an intermediate 'plateau' instead of region III, followed by a steep increase in concentration of particles near the bottom. A similar trend (even at lower velocities) is observed if the initial volume fraction is increased beyond those analysed so far (figure 9(c)). At lower velocities the plateau is quite extended, but it disappears if the rotor speed is high enough, leading to a very steep profile close to the bottom. At significantly higher velocities this sediment is simply compressed towards the bottom of the cell. The compressed profiles in figure 9, in which colloidal interactions must be quite significant, clearly fall outside the range of validity of equation (8). Further work will be needed to explain, for example, the peculiar plateau in figure 9.

4.2. Donnan potential measurements

Figure 10 shows a series of time-dependent measurements for determining the Donnan potential difference between the bottom and top fractions of a centrifuged silica dispersion

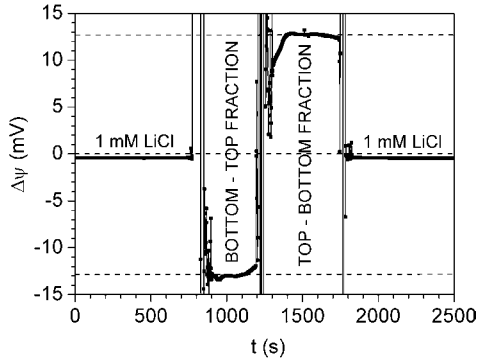

Figure 10. Measurements performed to determine the Donnan potential difference between a 1.3 vol% silica bottom fraction and a 0.12 vol% silica top fraction of a centrifuged silica dispersion in ethanol (background salt concentration ≈30 μM).

(see experimental details). Before and after measuring the sample dispersions, the potential difference was measured between the two calomel electrodes with 1 mM LiCl salt bridges contacting the same 1 mM LiCl solution; the resulting signal of -0.4 mV indicates that the two electrodes were almost identical and not altered due to contact with the sample dispersions (no electrical effect due to irreversible adsorption of silica particles, for example). The connections of the electrodes to the voltmeter were kept unchanged during the following measurements. The electrodes were removed from the LiCl solution ($t \approx 800$ s in figure 10) and introduced in a cell containing the bottom and top fractions obtained by centrifugation of the silica dispersion (see figure 2). The voltage indicates that the potential of the bottom fraction was -13 mV compared to the top fraction (the voltage went off scale for about 100 s, when the electrical circuit was open during transfer and ethanol rinsing of the electrodes). In the case of negligible or equal liquid junction potentials at the salt bridges, exchanging the electrodes between the two sample compartments should simply change the sign of the voltage, not the magnitude, and this was indeed observed ($t \approx 1200$ s in figure 10). A few minutes were required to obtain a constant voltage, after which its magnitude started to decrease, mainly because of the increasing salt concentration near the electrode inserted in the bottom fraction. In the time of the measurements in figure 10, the salt concentration of the sample dispersions increased by about 5%. From the measurement in figure 10, it is concluded that the difference in Donnan potential between the bottom and top fractions is -12.9 ± 0.5 mV.

The measured Donnan potential has the expected sign, negative like the surface charge of the colloidal silica particles. The value is also plausible compared to the theoretical prediction of -9 mV calculated from equations (6) and (7), where $z \approx 50$ is the colloid charge from electrophoresis, $\rho \approx 0.49$ μM at the bottom (1.3 vol%) and $\rho \approx 0.046$ μM at the top (0.12 vol%), and $c_s \approx 30$ μM (salt concentration determined for the top fraction). As expected, the Donnan potential was found to decrease upon increasing the salt concentration c_s at constant silica concentration or upon decreasing the silica concentration ρ at constant salt concentration. For instance, similar amounts of LiCl were added to the two compartments studied in figure 10, using the steady stream of LiCl solution from two salt bridges, and this led to an increase of the salt concentration of the top fraction compartment by about a factor of 4 and a decrease of the Donnan potential by a similar factor (it became -3 mV). When the silica concentration was decreased by a factor of 2, by mixing the two dispersions of figure 10, the Donnan potential difference with the initial top fraction also decreased by a factor of 2.

The influence of the salt bridge concentration on the Donnan potential measurements was studied systematically. Salt bridge concentrations below 1 mM LiCl did not lead to the

correct sign of the Donnan potential and also were clearly unreliable for other reasons. With 10 μM LiCl salt bridges, the potential oscillated, an effect related to the high resistivity of the system. With 100 μM LiCl salt bridges, switching the two calomel electrodes between the two dispersion compartments not only changed the sign but also the magnitude of the measured voltages, by several millivolts. These observations agree with the recommendation that a salt bridge should be much more concentrated than a sample dispersion under study [18–22], in this case much more than 30 μM. Using salt bridges with 1, 10, and 100 mM LiCl, the sign and magnitude of the measured Donnan potential were as shown in figure 10. However, the higher the salt bridge concentration, the faster the magnitude decreased due to contamination from the leaking salt bridge. This means that with salt bridges containing 100 mM LiCl or more, a reliable value of the Donnan potential as in figure 10 could not always be obtained.

5. General discussion

We have shown in section 4.1 that the SD-profiles of samples with an initial volume fraction between 0.045% and 0.48% exhibit all three predicted regions [5] and that the profiles could be very well fitted with equations (10)–(12), derived from the non-barometric formula (8). There is, nevertheless, a quantitative discrepancy: the charge determined from region II agrees in order of magnitude with that obtained from electrophoretic mobility measurements, but the charge $z^{(\mathrm{III})}$ determined from region III of the profiles is much lower and rather agrees with that obtained from the ratio $y(r_2)/y(r_1)$, according to equation (13). Several factors may contribute to, or account for, this discrepancy:

(a) deviation from the model in section 2 which relates the electric field to the particle number density (6), only on the basis of the neutrality condition (5),
(b) size polydispersity of particles,
(c) counterion condensation on colloids in region III (where both particle and counterion concentration are relatively high) or any other mechanism which makes z concentration dependent,
(d) colloid or ionic interactions, beyond the level assumed in equation (8).

With respect to (a), it should be noted that equation (6) for the electrostatic potential assumes local charge neutrality, i.e., it ignores charge inhomogeneities that are certainly present on a length scale comparable to the Debye length. A more elaborate version of the theory would relate the electric charge density $\rho_{\mathrm{EL}}(r)$ to the electric field gradients by $\nabla \cdot E(r) = \rho_{\mathrm{EL}}(r)/\varepsilon_0$. This was actually done in [5], where it was shown that the charge density may be nonzero over macroscopic distances in the vicinity of the crossover from one region to another. In these crossover regions the electric field is not constant, and therefore it affects the density profile.

Neglecting size polydispersity might indeed lower the determined value $z^{(\mathrm{III})}$: we used L_ω obtained from region I for charge determination. If this value of L_ω is replaced with a smaller value which would correspond to larger particles of the determined size distribution, $z^{(\mathrm{III})}$ could roughly increase by a factor of 2. However, the size polydispersity is, for given surface charge density, accompanied by charge polydispersity, which opposes the particle separation with different sizes in the centrifugal field, because it is the charge-to-mass ratio that counts. The electric force acting on larger particles with higher charge is also stronger and pushes the particles to the top of the region II. There are no noticeable changes, however, in the centrifugal length along region III (except of the 0.48% sample as discussed in the previous section), so it is unlikely that size polydispersity has a substantial effect on the value of $z^{(\mathrm{III})}$.

In the case (c) the discrepancy between z from electrophoresis measurements and $z^{(\mathrm{III})}$ may be explained as follows: electrophoresis employs an external field which pulls the opposite

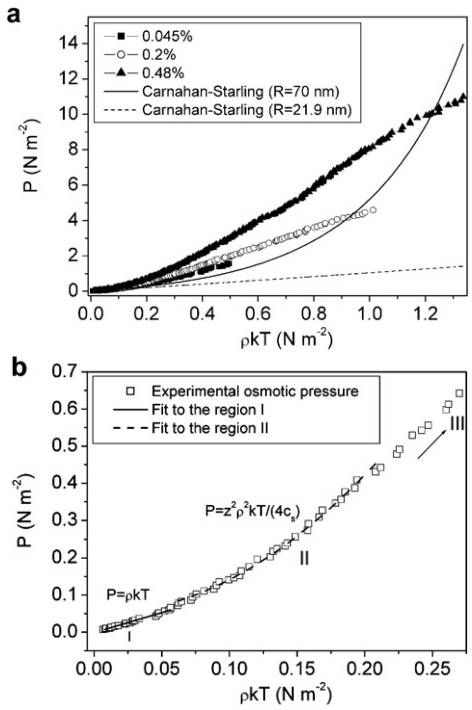

Figure 11. (a) Experimental osmotic pressures determined from the measured SD profiles for three different volume fractions of SiA dispersion and the calculated osmotic pressure using equation (19). (b) Determined osmotic pressure for the 0.045% sample at low particle number density and fits to region I and II with the indicated functions. (c) Determined osmotic pressure for the 0.2% sample and calculated osmotic pressures within three different approximations for $z = 34$. The inset contains the calculated osmotic pressures with the 'full linear theory' (see the text) for different values of z. (d) The same as (c) but for the case of the 0.48% sample and $z = 40$.

charges apart while in the centrifuge there is only attraction between colloids and counterions which may lead to counterion condensation and charge decrease. However, the change from $z^{(\mathrm{II})}$ to $z^{(\mathrm{III})}$ is too abrupt (at the crossover between the two regions), which is hard to be explained in this way. Concentration dependence of the charge z on the silica particles is certainly a realistic option. For silica the surface charge is due to adsorption of OH^- or a release of protons by –SiOH groups. This surface charge is known to depend on ionic strength [34] but may also be influenced by other colloids. Biesheuvel [35] recently incorporated the effect of this latter 'charge regulation' on SD-profiles and concludes that, at the higher volume fractions ($\phi > 0.1\%$), it improves data fits in comparison to the constant-charge model of section 2.

With respect to the effect of colloid–colloid interactions on SD-profiles, it is important to notice that in the derivation of equation (8) they are not *a priori* excluded. The equilibrium condition equation (4) for the colloids not only contains the ideal $\mathrm{d}\rho/\mathrm{d}r$ term, but also the ρ-dependent electrical field E, which is responsible for the inverse hyperbolic sine term in equation (8). Stated differently, the logarithmic (barometric) term in equation (8) is equivalent to van't Hoff's law $P = \rho kT$ for non-interacting, uncharged point particles and any additional (non-linear) ρ-term is a correction to this law and therefore somehow harbours an interaction effect. For example, in region II (figure 11(b)) a quadratic virial term appears in the osmotic pressure. Its interpretation, which is not straightforward, requires an analysis of the Donnan

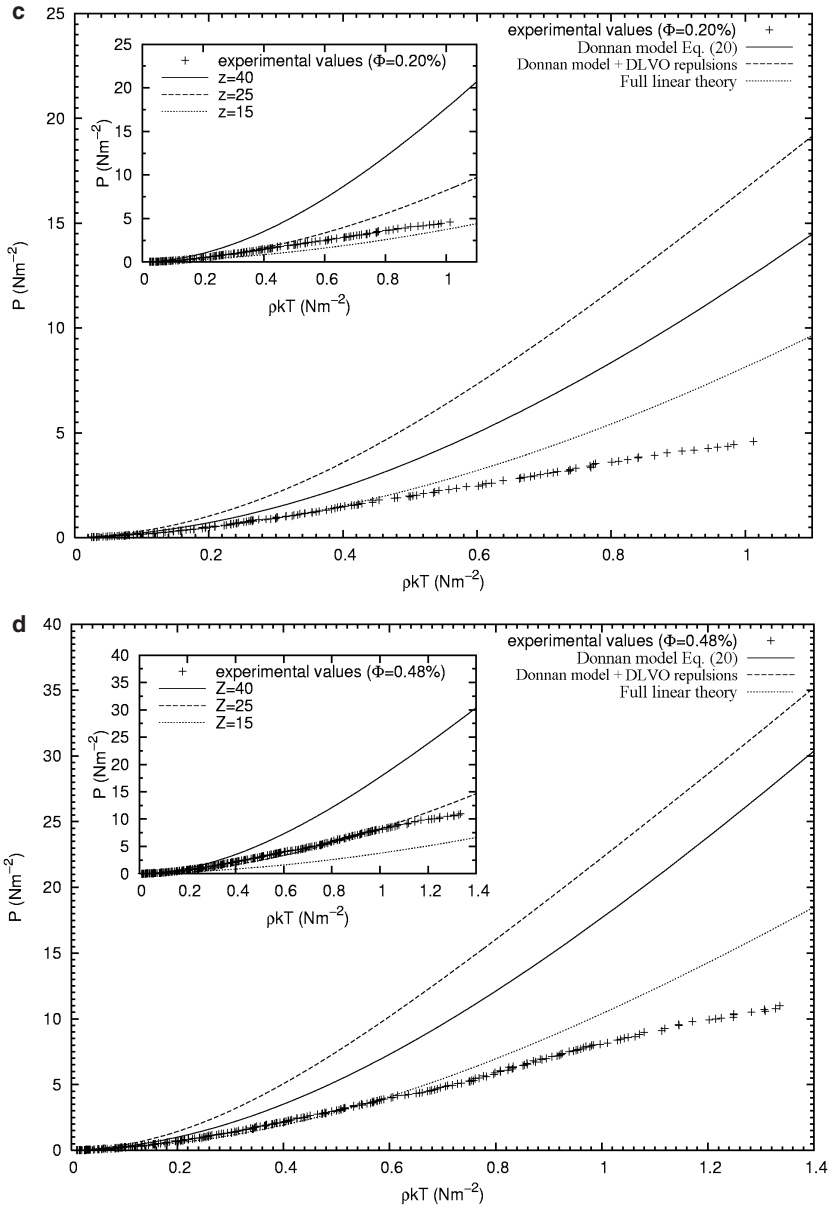

Figure 11. (Continued.)

equilibrium which is beyond the scope of this paper. We refer here to elaborate studies of osmotic pressures in the framework of the Donnan membrane equilibrium [36–39]. Here we will merely compare our data to various osmotic pressure calculations and specify in each case which interactions are included in the free energy.

Figure 11(a) shows osmotic pressures directly obtained from SD-profiles, determined by numerical integration, according to [7]. In the case of a centrifugal field the force balance on

the colloids reads: $\mathrm{d}P/\mathrm{d}r = m\omega^2 r\rho(r)$. Hence, the pressure follows from:

$$P = \frac{kT}{L_\omega^2}\int_{r_{\mathrm{top}}}^{r} x\rho(x)\,\mathrm{d}x, \tag{18}$$

where r_{top} is the radial coordinate at the top of the profile where $\rho \approx 0$, P is the osmotic pressure for the colloid number density $\rho(r)$ at radial coordinate r, and x is the integration (radial) variable. It should be noted that the resulting equation of state $P = P(\rho)$ is equivalent to the SD-profile without any additional assumptions about the colloid interactions. The results, however, are influenced by the chosen value for L_ω (taken from table 2 in our case). The results for three samples are presented in figure 11(a). The apparent differences in charge and ion concentration between these samples may lead to distinct curves in the corresponding regions II and III. All three regions can be easily identified by comparing the data to the equations for osmotic pressure in the various regions as derived in [5]. For the 0.48% sample, the region III is clearly the dominant one (and slightly distorted according to the discussion on the corresponding profile). In figure 11(b), regions I and II together with their linear and quadratic fits as predicted in [5], respectively, are presented for the 0.045% sample.

To further analyse the experimental osmotic pressure we first attempt an effective hard-sphere model using the Carnahan–Starling equation [30]:

$$P = \rho kT\frac{1+\Phi+\Phi^2-\Phi^3}{(1-\Phi)^3}, \tag{19}$$

i.e., the well-known semi-empirical equation of state for uncharged hard spheres. It is evident from figure 11(a), as expected, that the colloid charge substantially increases the osmotic pressure in comparison to the case of hard spheres. This increase, however, cannot be modelled with an effective diameter: a rescaling of the hard-sphere radius to $R + \kappa^{-1}$ in the Carnahan–Starling equation of state to match the experimental pressure generally fails. Figure 11(a) shows a typical example of discrepancy between the pressure of effective hard spheres and our charged silica spheres.

In figures 11(c) and (d), the experimentally determined osmotic pressure is compared to a theoretical equation of state calculated within three different approximations. The value of z considered for calculation is the corresponding value $z^{(\mathrm{II})}$ for each sample, given in table 2.

The first approximation is the Donnan model for the osmotic pressure [5, 8, 36–39]:

$$P = kT(\rho + c_+ + c_- - 2c_{\mathrm{s}}), \tag{20}$$

with c_+ and c_- given in terms of Donnan potential by equation (3), and the Donnan potential in terms of colloid density and reservoir salt concentration by equations (6) and (7). The Donnan model clearly overestimates osmotic pressures. The model applies to the osmotic pressure of an electroneutral bulk phase with a homogeneous distribution of all ions [36–39]. Thus all local details of the distribution of ions and electrical potentials are disregarded (just as in section 2) which presumably contributes to the discrepancy between the Donnan model and our data in figure 11(a).

In the second approximation, the effect of explicit pairwise repulsions between the colloids are added to the Donnan pressure of equation (20). These repulsions consist of hard-sphere and screened-Coulomb (DLVO) interactions. This combination of pressure contributions may appear natural at first sight but is actually somewhat naive: colloid–colloid interactions have already been taken into account implicitly in the Donnan equilibrium through the (mean-field) Donnan potential, so that some double counting of the colloidal repulsions takes places (this will be corrected in the third approximation below). We employ here the Gibbs–Bogolyubov inequality to obtain the Helmholtz free energy of the DLVO dispersion on the basis of an effective hard-sphere reference system as described in [31]. The osmotic pressure contribution

then follows from a volume derivative of the free energy. We assume that the Debye screening length that determined the range of the interactions depends on the colloid density (due to the variation in salt concentration), yielding an additional volume dependence of the free energy and hence an extra osmotic pressure contribution.

In the third approximation, the Donnan osmotic pressure as well as the hard-sphere and screened-Coulomb repulsions are taken into account, as in the second approximation. However, we now also include so-called volume terms to the total free energy, which have been argued to be relevant for systems with low ion concentrations [31, 32]. One of these volume terms consists of the ideal-gas free energy of the salt ions, and gives rise to an ionic osmotic pressure contribution as in equation (20), i.e., it has already been taken into account in the first and second approximation. The most important new volume-term contribution that is taken into account in the third approximation involves the (density-dependent) self-energy of the colloids due to the double layer potential well in which they reside. The remaining contributions to the volume terms describe (a) the effects of the exclusion of ions from the cores of the particles and (b) corrections for the mean-field contributions of the colloidal DLVO repulsions. The last term originates from the average electric potential due to the ions, which almost cancels the mean-field potential due the colloids because of charge neutrality. In other words, the so-called 'full linear theory' includes the Donnan pressure comprising also the ideal van't Hoff law, the DLVO repulsions, and the effect of all the remaining volume terms. The exact expression used for the volume terms is the grand-canonical version of expression (61) of [31], which will be discussed and derived in detail elsewhere [33]. It can be seen in figures 11(c) and (d), where the osmotic pressures that results from the 'full linear theory' are shown, that the addition of all the volume terms accounts for a significant decrease in the osmotic pressure compared to the pressure within the one-component 'DLVO' picture. This might provide part of the explanation for the much too low charge determined from region III on the basis of the Donnan model, and is a topic for future work.

It can also be observed from figures 11(c) and (d) that the region II of the experimental osmotic pressure has a smaller spatial extension than the predicted one, which leads to a smaller slope of the linear region III of the determined pressure and results thus in the underestimation of $z^{(\mathrm{III})}$. The insets of these two figures show the 'full linear theory' calculated for different values of z. Even though the values of the calculated pressure at lower z are closer to the data in region III, the shape of the calculated pressure does not match that of the data and the overall agreement with the data cannot be seen. There is very likely more than one phenomenon to be considered in order to explain the discrepancies discussed in this section.

It should be noted that the electrochemically measured Donnan potentials correspond to the macroscopic electrical potential, irrespective of interparticle interactions. The measurements agree in sign and order of magnitude with voltages expected on basis of the UC profiles (figure 8(a)) and with Donnan potentials calculated from the colloid and salt concentrations in the electrochemical cell and from the electrophoretically determined charge of $z \approx 50$.

A further confirmation of the presence and effects of the internal electric field in SD-profiles can be found in the recent confocal microscopy study of Royall *et al* [40] on latex dispersions.

6. Conclusions

We have experimentally demonstrated the existence of a macroscopic electric field, producing strongly non-barometric sedimentation–diffusion (SD) profiles of charged colloidal dispersions. The unusual shape of experimental SD-profiles and its sensitivity to added salt agree qualitatively with equation (8) (and its asymptotic forms equations (10)–(12)).

The region II of the profiles yields a value of the number of elementary charges per particle which agrees in order of magnitude with the value estimated from electrophoresis. Even though in region III the electric field is also expected to dominate the profiles, the obtained value of z is significantly lower than expected from electrophoresis and than in region II.

Several factors may account for the deviation from the 'non-barometric' SD-profile according to equation (8): inter-particle repulsive interactions of the DLVO type and the volume terms, counterion condensation, effect of details on electric field on the scale of ions and particles, and particle size polydispersity. It seems that in particular the volume terms in the free energy, which significantly decrease the osmotic pressure, may partly account for the small values of z obtained from region III. Also charge regulation [35] likely suppresses to some extent the determined particle charge. Clearly further theory is needed to improve the quantitative analysis of the experimental SD-profiles beyond equation (8). The electrical potential difference between the top and bottom of SD-profiles, estimated on the basis of equation (8), nevertheless agree quite well with direct electrochemical measurement on silica dispersions, assuming the particle charge of $z \approx 50$ which is also found from electrophoresis.

At silica volume fractions exceeding 0.5%, the shape of the profiles, measured at the same centrifugal field as for lower volume fractions, completely deviates from the profile predicted by equation (8). To elucidate these marked deviations clearly requires future experimental and theoretical study of concentrated regions of SD-profiles, which may contain important information about interacting charged colloids.

Acknowledgments

Nathalie Zuiverloon synthesized the silica spheres and Dr Dominique Thies-Weesie is acknowledged for advice and support with respect to the analytical ultracentrifuge. Professor A Vrij is thanked for his interest and the useful discussions on charged colloids. This work was financially supported by The Netherlands Organization for Scientific Research (NWO—Stichting Chemische Wetenschappen). The work of co-authors R van Roij and B Zoetekouw is part of the research program of the Stichting voor Fundamenteel Onderzoek der Materie (FOM), which is financially supported by NWO.

References

[1] Perrin J 1913 *Les Atomes* (Paris: Alcan)
[2] Biben T and Hansen J P 1994 *J. Phys.: Condens. Matter* **6** A345–9
[3] Löwen H 1998 *J. Phys.: Condens. Matter* **10** L479–85
[4] Philipse A P and Koenderink G H 2003 *Adv. Colloid Interface Sci.* **100–102** 613–39
[5] van Roij R 2003 *J. Phys.: Condens. Matter* **15** S3569–80
[6] Hynninen A P, van Roij R and Dijkstra M 2004 *Europhys. Lett.* **65** 719–25
[7] Piazza R, Bellini T and Degiorgio V 1993 *Phys. Rev. Lett.* **71** 4267–70
[8] Philipse A P 2004 *J. Phys.: Condens. Matter* **16** S4051–62
[9] Raşa M and Philipse A P 2004 *Nature* **429** 857–61
[10] Chen F F 1984 *Introduction to Plasma Physics* (New York: Plenum)
[11] Philipse A P and Vrij A 1988 *J. Chem. Phys.* **88** 6459–70
[12] Thies-Weesie D M E, Philipse A P, Nägele G, Mandl B and Klein R 1995 *J. Colloid Interface Sci.* **176** 43–54
[13] Pathmamanoharan C and Philipse A P 1994 *J. Colloid Interface Sci.* **165** 519
[14] Overbeek J Th G 1953 *J. Colloid Sci.* **8** 593
[15] Overbeek J Th G 1969 *Colloid Science* ed H R Kruyt (Amsterdam: Elsevier)
[16] Lyklema J 1991 *Fundamentals of Interface and Colloid Science* vol 1 (New York: Academic)
[17] Atkins P and de Paula J 2002 *Atkins' Physical Chemistry* 7th edn (Oxford: Oxford University Press)
[18] Sawyer D T and Roberts J C Jr 1974 *Experimental Electrochemistry for Chemists* (New York: Wiley)
[19] Westcott C 1978 *pH Measurements* (New York: Academic)

[20] Bard A J and Faulkner L R 1980 *Electrochemical Methods, Fundamentals and Applications* (New York: Wiley)
[21] Mac Innes D A 1961 *The Principles of Electrochemistry* (New York: Dover)
[22] Hiemenz P C 1977 *Principles of Colloid and Surface Chemistry* (New York: Dekker)
[23] Bockris J O'M and Reddy A K N 1970 *Modern Electrochemistry* vol 2 (London: MacDonald)
[24] Hills G J 1961 *Reference Electrodes, Theory and Practice* ed D J G Ives and G J Janz (New York: Academic) chapter 10
[25] Hills G J and Ives D H G 1961 *Reference Electrodes, Theory and Practice* ed D J G Ives and G J Janz (New York: Academic) chapter 3
[26] Danner P S 1922 *J. Am. Chem. Soc.* **44** 2832
[27] Verwey E J W and Overbeek J Th G 1999 *Theory of the Stability of Lyophobic Colloids* (New York: Dover)
[28] Rasa M, Philipse A P and Meeldijk J D 2004 *J. Colloid Interface Sci.* **278** 115–25
[29] Philipse A P and Vrij A 1989 *J. Colloid Interface Sci.* **128** 121–53
[30] Carnahan N F and Starling K E 1969 *J. Chem. Phys.* **51** 635
[31] van Roij R, Dijkstra M and Hansen J-P 1999 *Phys. Rev.* E **59** 2010–25
[32] Warren P 2000 *J. Chem. Phys.* **112** 4683
[33] Zoetekouw B and van Roij R 2005 to be submitted
[34] Iler R K 1979 *The Chemistry of Silica* (New York: Wiley)
[35] Biesheuvel P M 2004 *J. Phys.: Condens. Matter* **16** L499–504
[36] Hill T L 1956 *Discuss. Faraday Soc.* **21** 31
[37] Stigter D 1960 *J. Phys. Chem.* **64** 838
[38] Hill T L 1986 *An Introduction to Statistical Thermodynamics* (New York: Dover)
[39] Vrij A 1990 *Colloids Surf.* **51** 299
[40] Royall C P, van Roij R and van Blaaderen A 2004 *J. Phys.: Condens. Matter* submitted